https://doi.org/10.1016/j.jsv.2016.03.011

Estimation of source location and ground impedance using a hybrid multiple signal classification and Levenberg-Marquardt approach

Kai-Chung Tam[a], Siu-Kit Lau[b], Shiu-Keung Tang[a,*]

[a]Department of Building Services Engineering,
The Hong Kong Polytechnic University,
Hong Kong
China

[b]Department of Architecture
National University of Singapore,
4 Architecture Drive,
Singapore, 117566

[a)] Author to whom correspondence should be addressed.
Electronic mail: shiu-keung.tang@polyu.edu.hk

Abstract

A microphone array signal processing method for locating a stationary point source over a locally reactive ground and for estimating ground impedance is examined in detail in the present study. A non-linear least square approach using the Levenberg-Marquardt method is proposed to overcome the problem of unknown ground impedance. The multiple signal classification method (MUSIC) is used to give the initial estimation of the source location, while the technique of forward backward spatial smoothing is adopted as a pre-processer of the source localization to minimize the effects of source coherence. The accuracy and robustness of the proposed signal processing method are examined. Results show that source localization in the horizontal direction by MUSIC is satisfactory. However, source coherence reduces drastically the accuracy in estimating the source height. The further application of Levenberg-Marquardt method with the results from MUSIC as the initial inputs improves significantly the accuracy of source height estimation. The present proposed method provides effective and robust estimation of the ground surface impedance.

1. Introduction

The use of phased-array microphone system for the investigation of acoustic problems has been rapidly growing in past decades because of the advancement of multichannel electronic instruments and digital signal processing. It is a powerful tool for characterization of sound sources when it is applied together with a proper sound propagation model and an optimal array-processing algorithm. Its applications include acoustic source localization, tracking, strength estimation, signal enhancement and etc. (for instance, Refs. [1]-[7]). The selection of the signal processing algorithm is in general based on prior knowledge and proper assumptions of the sound propagation model. A time-harmonic point source is a widely adopted model because of its simplicity for implementation. It can also be interpreted as a basic component of more complex acoustic sources.

Delay and sum (DAS) beamforming method is a fundamental array processing technique [[8]-[11]], which can extract the direction of arrivals (DOA) and source strength of uncorrelated sources from given array signals. Difference enhancement methods [[12],[13]] have been developed for improvement of spatial resolution and reduction of sidelobe contribution from DAS. Minimum variance distortionless response (MVDR) [[14]-[16]] is one of the best known improved methods, which makes use of desired constraints, to minimize the sidelobe contribution from other directions and to retain the response from the desired direction. Besides the MVDR method, deconvolution methods [[10],[12],[17]-[22]] have been developed for reduction of sidelobe contribution based on deconvolution of the DAS beamformer output by its filtering response function. The individual source strength can be restored with sufficient steps of iteration. A notable improvement can be found in the source strength estimation with multiple sources using deconvolution methods [[17],[23]]. However, the deconvolution algorithm can only remove the contamination from uncorrelated sources in the expense of large computational power.

In the presence of coherent sources, the deconvolution method cannot be directly applied because the transfer function of the source pair is usually unknown. They will also bias the predictions of arrival direction and source strengths, if incoherent sources are assumed. Failure of the MVDR method in the presence of coherent sources is caused by a reduced rank of the signal correlation matrix, which makes collapse of the optimized solutions in the incoherent case. To overcome this problem without priori-knowledge of the coherence between sources, spatial smoothing method [[16], [24]-[26]] is proposed to provide a fast and simple computation. The major drawback of spatial smoothing is the requirement of a pre-design sub-array with regular spacing and thus loss of effective array geometry [[27]]. This may also reduce the spatial resolution and narrow the frequency bandwidth. Though the DOA in the presence of coherent sources may be recovered using spatial smoothing method by restoring the rank of the matrix, the strength of the primary source may not be fully recovered because the directional response of the secondary source still contributes to the focused directional response of the primary source. Complete rejection of the secondary source's contributions by null steering method [[9], [27]-[30]] may be needed.

Coherent sound sources are common in the outdoor environments. The interfering coherent sources can be caused by the ground or façade/wall reflections. These reflections are time delayed and attenuated versions of the direct sound. Li et al. [[31]] has studied the source height determination with the horizontal separation between the point source and the receiver a priori knowledge. The ground impedance is estimated using signals from two microphones with an assumed ground impedance model. Kruse and Taherzadeh [[32]] have investigated the effects of environmental conditions on the source distance and height estimation using a vertical sensor array. However, ground impedance is an input to their scheme and thus a ground impedance model is again required. It should be noted that the

estimation of ground impedance will become relatively straight-forward when the source position is known (for instance, Refs. [33] - [35]).

To predict the DOA of sound sources without considering their relative source strength and their ranges from the receivers, high-resolution eigen-based approach is a widely adopted method. The multiple signal classification method (MUSIC) [[36]] is based on the decomposition of signal vectors into signal and noise subspaces. Its easy implementation and high spatial resolution make MUSIC method widely adopted. In the presence of coherent sources, MUSIC can be used to estimate DOA with pre-processing of spatial smoothing [[24]].

In this study, a hybrid method combining MUSIC and the Levenberg-Marquardt approach is proposed for improved source location estimation in the presence of coherent ground reflection and for predictions of ground impedance. For simplicity, sound propagation due to a time-harmonic point source at rest over an impedance ground surface is considered. Once the source locations are identified, the impedance of the reflecting ground surface can be estimated. Unlike the case of Li et al. [[31]] and similar studies, the present proposed method will estimate source location and ground impedance directly without adopting any ground impedance model and without prior knowledge of the source range.

2. Recovery of source and ground characteristics

A non-linear least square approach to estimate the location of a stationary sound source and ground surface impedance is proposed in the present study. It is achieved through three steps: (1) the measured signals are processed with forward-backward spatial smoothing (FBSS) to eliminate as far as possible the interference from the coherent reflection; (2) MUSIC method is used to give an initial estimation of the source location and (3) the closest estimated source location will be traced by the Levenberg-Marquardt (LM) method [[37],[38]]

which is a non-linear least square based iterative method. Ground surface admittance will be estimated by the LM method. Details of the methodology will be discussed in this section.

2.1. Sound wave propagation model

2.1.1. Outdoor sound propagation over an impedance ground surface

Figure 1 shows the present sound propagation model above a flat impedance ground surface. The plane $z = 0$ is the ground surface, while the origin of the coordinate system is placed at an arbitrary location on the horizontal $z = 0$ plane. The observation point is at $\mathbf{x}_m = (x_m, y_m, z_m)$, while a point monopole source and its image are located at $\mathbf{x}_s = (x_s, y_s, z_s)$ and $\mathbf{x}_i = (x_s, y_s, -z_s)$ respectively. Chien and Soroka [[39]] developed an approximate method for estimating the sound pressure field due to a point source over a locally-reacting surface. The total pressure, $P_t(\mathbf{x}_m,\mathbf{x}_s,Q)$, due to a monopole of unit strength at the observation point can be estimated by the superposition of the direct and reflected complex sound pressures:

$$P_t(\mathbf{x}_m, \mathbf{x}_s, Q) = \frac{e^{-j(\omega t - kr_1)}}{4\pi r_1} + Q\frac{e^{-j(\omega t - kr_2)}}{4\pi r_2}, \tag{1}$$

where r_1 and r_2 are the distances of the direct and reflected paths respectively, k is the wavenumber and $j = \sqrt{-1}$. The first and second terms on right-hand-side of Eq. (1) represent the complex sound pressures due to the source and the ground reflection respectively. In the present study, the beamforming method is evaluated based on and limited to the grazing incidence. For grazing incidence, the spherical wave reflection coefficient Q can be expressed as:

$$Q \approx R_p + (1 - R_p)F(w_{nd}), \tag{2}$$

where $F(w_{nd})$ is the boundary loss factor given as:

$$F(w_{nd}) = 1 + j\sqrt{\pi} w_{nd} e^{-w_{nd}^2} \operatorname{erfc}(-jw_{nd}), \tag{3}$$

and erfc(·) represents the complementary error function. w_{nd} denotes the numerical distance:

$$w_{nd} = \sqrt{\frac{jkr_2}{2}}(\cos\theta + \beta), \tag{4}$$

where β is the specific normalized surface admittance and θ the incident angle. R_p is the plane wave reflection coefficient of the ground surface given as:

$$R_p = \frac{\cos\theta - \beta}{\cos\theta + \beta}. \tag{5}$$

2.1.2. Generalized coherent point-sources model

The spherical wave reflection coefficient in Eq. (1) is a function of spatial differences between source and receivers. The received signals of N number of microphones at frequency ω due to a single point source above an impedance surface can be expressed as:

$$\mathbf{S}(\omega) = a \cdot \begin{bmatrix} P_t(\mathbf{x}_1, \mathbf{x}_s, Q) \\ P_t(\mathbf{x}_2, \mathbf{x}_s, Q) \\ \vdots \\ P_t(\mathbf{x}_n, \mathbf{x}_s, Q) \\ \vdots \\ P_t(\mathbf{x}_N, \mathbf{x}_s, Q) \end{bmatrix}, \tag{6}$$

where a denotes the constant source strength of a stationary source. The estimated sample covariance matrix $\hat{\mathbf{R}}(\omega)$ can be expressed as:

$$\hat{\mathbf{R}}(\omega) = \mathbf{S}(\omega)\mathbf{S}(\omega)^H. \tag{7}$$

$\hat{\mathbf{R}}(\omega)$ contains the signal relationship in spatial domain between microphones. The superscript H denotes conjugate transpose. The present proposed method will be based on the extraction of source properties from $\hat{\mathbf{R}}(\omega)$ and $\mathbf{S}(\omega)$. The symbols with hat hereinafter denote estimated values in the present study.

2.2. Recovery of stationary source strength and ground characteristics

2.2.1. Parameter estimation

A non-linear least square approach is adopted for the estimation of source properties and ground impedance in the frequency domain. We define the error vector $\mathbf{e}(\omega)$ as:

$$\mathbf{e}(\omega) = \left[\mathbf{S}(\omega) - \hat{\mathbf{S}}(\omega)\right], \tag{8}$$

where $\mathbf{S}(\omega)$ and $\hat{\mathbf{S}}(\omega)$ are the reference and estimated signal vectors, respectively. As shown in Eq. (1), $\mathbf{S}(\omega)$ consists basically of three unknown parameters namely $\mathbf{x}_s$, $\mathbf{x}_m$, and Q. In the present study, the plane of the microphone array is set to be parallel to a vertical plane containing the sound source and its image (i.e. the plane $y = y_s$). The perpendicular distance of the array centre to this vertical plane, y_s, is known with $y_m = 0$. This situation is common in towns where sound sources are embedded in a linear row of houses and buildings, but their positions in the x- and z-direction are not exactly known. The unknowns left in the estimation of $\mathbf{S}(\omega)$ are x, z, and β, which are the horizontal distance of the source from the x-axis, source height above ground and the admittance of the ground surface respectively. $\hat{\zeta}$ is the estimated parameter vector:

$$\hat{\zeta} = \left[\hat{x} \quad \hat{z} \quad \hat{\beta}\right], \tag{9}$$

which will be estimated in the process. The objective of the optimization process is to minimize the cost function of the error vector. In the present study, l^2-norm of error vector is used as the cost function. An extended version of Gauss-Newton method, called Levengerg-Marquardt (LM) method, is adopted for the optimization process in order to provide fast optimization.

Levenberg-Marquardt method is a modified version of the well-known Gauss-Newton method by introducing a regulating parameter in the optimization process [[37],[38]]. The optimization criteria are on minimizing the error vector e between the measured data vector

and the modal signal vector. The gradient operator with respect to parameter vector is a ($N \times L_s$) Jacobian matrix, as:

$$\mathbf{J}(\omega) = \left[\frac{\partial \mathbf{e}(\omega)}{\partial x} \quad \frac{\partial \mathbf{e}(\omega)}{\partial z} \quad \frac{\partial \mathbf{e}(\omega)}{\partial \beta} \right], \tag{10}$$

where L_s is the total number of sub-array. The computation of the Jacobian matrix is performed numerically by backward finite difference method. The updating process of LM method for the $(b+1)^{\text{th}}$ estimate of the parameter vector $\hat{\zeta}_{b+1}$ is [[37],[38]]:

$$\hat{\zeta}_{b+1} = \hat{\zeta}_b - \left\{ \mathbf{J}_b(\omega)^T \mathbf{J}_b(\omega) + \lambda_d \operatorname{diag}\left[\mathbf{J}_b(\omega)^T \mathbf{J}_b(\omega) \right] \right\}^{-1} \mathbf{J}_b(\omega)^T \mathbf{e}_b(\omega), \tag{11}$$

where $\mathbf{J}(\omega)$ is the Jacobian matrix of the measured signals and λ_d is a positive scalar regularization parameter. The subscribe b indicates the number of iterations. The LM method is identical to the Gauss-Newton method when $\lambda_d = 0$. The selection of λ_d influences the rate of convergence to the solution. λ_d can be either a constant or variable updated adaptively with respect to the cost function. In the present study, λ_d is set at 0.01 for the stability of estimation.

An initial estimate of the parameter vector ζ is required before the optimization process. Similar to the Gauss-Newton method, a close initial estimate of ζ will lead to a faster convergence rate and reduce the chance of bias estimation. Since the cost function is non-convex and sensitive to the initial estimation, a high precision eigen-value based location estimation method is needed to give the initial estimate of ζ. In this study, MUSIC is used to give such location estimation. In order to implement MUSIC with coherent sources, a pre-processing forward-backward spatial smoothing (FBSS) method is used. MUSIC and FBSS will be discussed in next sub-sections.

The l^2-norms of the error vector shown in Eq. (8) are calculated using the source location estimated by MUSIC together with a series of β estimated by ground parameters

(shown later) ranging from low to high values in regular increment intervals. The β which results in the smallest error vector l^2-norm is taken to be the initial β for the LM procedure.

2.2.2. Initial estimation of source location with coherent source by MUSIC

MUSIC is a popular eigen-structure based method in spectrum analysis [[36]]. This method has been proved a high resolution method in DOA estimation of sound sources [[40] -[43]]. MUSIC extracts the signal and noise subspaces from the covariance matrix. The subspaces estimation is based on eigenvalue decomposition of the covariance matrix. The DOA of the source is estimated by the orthogonal properties of noise subspace vector and the array manifold vector. A correct estimation of the subspaces required that the noise and the desired signals are uncorrelated with each other.

To overcome this limitation of MUSIC, spatial smoothing technique to de-correlate the desired signals is proposed. Also, microphone position transformation method is used to implement spatial smoothing technique with irregular array configuration. Without prior knowledge of ζ, the far field sound DOA will first be estimated by MUSIC. With the estimated azimuth and elevation angles, the range of the source will be further estimated by MUSIC with the near-field assumption. The proposed method for source localization is summarized as follows in this section.

Suppose there are D number of sound sources and N number of microphones. In reality with uncorrelated background noise, Eq. (7) can be revised into a noisy sample covariance matrix as:

$$\hat{\mathbf{R}}_{noisy} = \mathbf{S}(\omega)\mathbf{S}(\omega)^H + \alpha_n^2\mathbf{I}, \tag{12}$$

where α_n and $\mathbf{I}$ are strength of noise and unit matrix respectively. To estimate the signal and noise subspace, eignenvalues and eigenvectors are extracted from $\hat{\mathbf{R}}_{noisy}$ by eigenvalue decomposition. The $(N-D)$ number of eigenvectors (v_i, where i = 1 to $N - D$) are selected

with the associated $(N-D)$ number of smallest eigenvalues. For uncorrelated sources, the D number of largest eigenvalues represents the powers of the corresponding signals, while the $(N-D)$ smallest eigenvalues are equal to the variance of the noise. Therefore, a $N \times (N-D)$ dimensional subspace, which is spanned by the abovementioned $(N-D)$ eigenvectors as

$$\mathbf{E}_n(\omega) = \begin{bmatrix} v_1 & v_2 & v_3 & \dots & v_{(N-D)} \end{bmatrix} \tag{13}$$

can be created. The MUSIC pseudospectrum is given as:

$$\mathbf{P}_{MUSIC}(\omega,\varphi) = \left| \mathbf{A}(\omega,\varphi)^H \mathbf{E}_n(\omega) \mathbf{E}_n(\omega)^H \mathbf{A}(\omega,\varphi) \right|^{-1}, \tag{14}$$

where $\mathbf{A}(\omega,\varphi)$ is the array manifold vector of the phased-array microphone system [[36]]. Since the signal and noise subspaces are orthogonal to each other, $\mathbf{P}_{MUSIC}(\omega,\varphi)$ will reach a local maximum when the scanning DOA (i.e. φ) matches the DOA of a source.

A three-dimensional search using Eq. (14) is computationally inefficient. To achieve more effective source localization, the three-dimensional locations can be estimated in two stages. First, a far field plane wave modeled array manifold vector is applied to Eq. (14) to estimate the elevation and azimuth angle. Afterwards, the estimated angle is used for searching the range of the source (i.e. the distance between the source and receiver center) through a simple one-dimensional search implemented by MUSIC. In the second stage, a near field spherical wave modeled array manifold vector is used in Eq. (14).

2.2.3. De-coherence with spatial smoothing (SS) technique

The conventional MUSIC cannot be applied directly in the presence of coherent sources (e.g. source-reflection pairs). To solve this problem, the spatial smoothing (SS) technique is used. The SS technique is a preprocessing scheme to restore the rank of the array covariance matrix, since the matrix is rank-deficient in the presence of coherent source.

The forward-backward spatial smoothed sample array covariance matrix $\mathbf{R}_{FBSS}$ is used to replace the sample array covariance matrix $\hat{\mathbf{R}}_{noisy}$ in Eq. (12) [[44]]. It is done by de-correlating the coherent source signals by averaging sub-array covariance. With adaptive array processer that creates null at the unwanted signal direction, the coherence source signal can be eliminated.

The forward smoothing array covariance matrix $\mathbf{R}_f$ is the averaged covariance matrix over L_s sub-arrays given as [[36]]:

$$\mathbf{R}_f = \frac{1}{L_s}\sum_{l=1}^{L_s}\mathbf{R}_l^f , \tag{15}$$

where $\mathbf{R}_l^f$ denotes the covariance matrix (forward) of the l^{th} sub-array. Similarly, the backward smoothing array covariance matrix $\mathbf{R}_b$ is the averaged covariance matrix given as [[36]]:

$$\mathbf{R}_b = \frac{1}{L_s}\sum_{l=1}^{L_s}\mathbf{R}_l^b , \tag{16}$$

where $\mathbf{R}_l^b$ denotes the covariance matrix (backward) of the l^{th} sub-array. The resultant forward/backward spatial smoothed covariance matrix $\mathbf{R}_{FBSS}$ can be found by the average of the forward and backward sub-array covariance matrix as [[36]]:

$$\mathbf{R}_{FBSS} = \frac{\mathbf{R}_f + \mathbf{R}_b}{2} . \tag{17}$$

While L_s is much higher than the number of sources, the spatial smoothed covariance matrix $\mathbf{R}_{FBSS}$ can be rank-restored. It is noted that the number of microphones in each sub-array is less than that in the original array, thus the spatial resolution and effective aperture are reduced. The number of microphones in and the geometry of each sub-array must be

identical for the pre-processing scheme as discussed in next section. In the present study, $\hat{\mathbf{R}}_{FBSS}$ replaces $\hat{\mathbf{R}}_{noisy}$ in Eq. (12).

2.2.4. Transformation of irregular array into regular rectangular array

One of the limitations of spatial smoothing (SS) preprocessing algorithm is the requirement of regular sub-array geometry. For signals with priori-known narrow-band frequency, the regular array has various benefits in installation and simpler processing due to symmetric geometry [[36]]. However, irregular array geometry has an advantage of wider accessible frequency of incoming signals [[45]]. For irregular array geometry, a virtual array covariance matrix $\mathbf{R}_v$ is required for the SS method. In the present study, a linear array interpolation technique [[24]] will be used and is discussed in this sub-section. It is a least square based linear transformation of array covariance matrix from non-uniform geometry into desired geometry.

Firstly, $\mathbf{A}_r$ and $\mathbf{A}_v$ denote the array manifold of a real arbitrary array and a virtual array with pre-designed microphone positions, respectively. The number of microphones in the virtual array should be less than or equal to that of the real array. It is assumed that the entire directional region of interest is divided into N_s number of sections. For the n_s^{th} section with angles between φ_{ns}^1 and φ_{ns}^2, where the superscripts 1 and 2 indicate the lower and upper bounds of the angles in the n_s^{th} section respectively, for the spatial smoothing algorithm. The region is further divided into sub-sections with angular interval $\Delta\varphi$. $\mathbf{A}_r(\varphi_{ns})$ and $\mathbf{A}_v(\varphi_{ns})$ corresponding to a set of angles $\left[\varphi_{ns}^1,\ \varphi_{ns}^1+\Delta\varphi,\ \varphi_{ns}^1+2\Delta\varphi,\ ...,\ \varphi_{ns}^2\right]$ are created. The relationship between the real and virtual array manifolds can be written as:

$$\mathbf{B}\mathbf{A}_r(\varphi_{ns}) = \mathbf{A}_v(\varphi_{ns}), \tag{18}$$

where **B** is the transfer matrix and can be found by least square method as:

$$\mathbf{B} = \frac{\mathbf{A}_v \mathbf{A}_r^H}{\mathbf{A}_r \mathbf{A}_r^H + \sigma_L \mathbf{I}}. \tag{19}$$

σ_L is an arbitrary loading factor. In the present study, $\sigma_L = 10^{-8}$. The virtual array covariance matrix $\mathbf{R}_v$ can be estimated by the real array covariance matrix $\hat{\mathbf{R}}_{noisy}$ and the transfer matrix **B** as:

$$\mathbf{R}_v = \mathbf{B}\hat{\mathbf{R}}_{noisy}\mathbf{B}^H. \tag{20}$$

By arranging the virtual array with uniform regular configurations, the spatial smoothing technique can be applied on any real array with arbitrary geometry. Figure 2 summarizes the numerical steps for the parameter estimation in this study.

3. Computer simulations

Numerical simulations are performed to investigate the performance of the abovementioned methods for source location and ground impedance estimations. A 36-channel microphone array with irregular microphone configuration designed by Brüel & Kjaer [[46]] is used (hereinafter referred to as real array). This array has wide frequency range for acoustic analysis from 500 Hz to 5000 Hz. Virtual array with the same number of microphones arranged in the form of a 6 × 6 equi-spaced rectangular matrix is set for spatial smoothing method. This arrangement aims to minimize the deviation of the horizontal and vertical resolutions of the direction responses. The spacing between virtual microphones varies with source sound frequency and is kept at half wavelength of the sound. The configurations of the real array and two virtual arrays are illustrated in Fig. 3.

Throughout the analysis, the centers of the arrays are located at 0.32 m above the ground surface. This ensures that the lowest microphone is just above the ground surface. FBSS with rectangular sub-array of a 4 × 4 microphone arrangement is applied. The configuration of the sub-array is to provide sufficient number of sub-array averaging for

source de-coherence. Allowing for overlapping elements between sub-arrays, a total 9 sub-arrays are used in the present study.

Three values of flow resistivity, σ_{eff}, have been used for the evaluation of ground surface impedance estimation. They simulate three practical situations of asphalt (σ_{eff} = 30 MNs/m^4), sandy silt (σ_{eff} = 2 MNs/m^4) and roadside dirt (σ_{eff} = 0.5 MNs/m^4) [[47]]. It is assumed that the entire ground is homogeneous. The ground surface is flat and assumed to be locally reacting with infinite thickness. There is also no other reflecting object in the sound propagation path between the source and receivers. Delany and Bazley's model [[48]] with the single parameter σ_{eff} is adopted for the calculation of β and $\mathbf{S}(\omega)$ for simplicity. Though this model may produce non-physical ground impedance spectra and may not be good for outdoor applications [[49]], it is used here just to create ground impedances for evaluation of the present proposed method and is not required for the LM procedure. It is believed that the conclusion is not affected by any impedance model adopted.

The sound source considered in the simulation is a harmonic point source above ground surface. Its strength is kept constant throughout the simulation. Uncorrelated Gaussian white noise with constant strength is added to the input signals as background interference. The signal-to-noise ratio (SNR) in the present study is defined as the power ratio of the primary source and the background noise in decibels.

For each case, the sample covariance matrix is determined in the frequency domain. The maximum number of iteration for the LM method is set at 100. The results with minimum mean squared error of the 100 iterations is selected as the final results for each simulation. The statistical results presented hereinafter are obtained from 1000 simulations for each case tested.

In this section, both the results for the initial estimation of source location by MUSIC and the results from LM optimization process are discussed. The percentage mean squared errors and their standard deviations are adopted as assessment parameters.

3.1. Results from MUSIC

The MUSIC location estimation is performed with a uniform grid searching in spherical coordinates. The unit spacing between the grid at both x-axis and z-axis is 0.001 radian. Since the distance from microphone array to ground surface is known, for the real source localization, only the pseudospectrum above ground surface will be computed. The peak of the spatial MUSIC pseudospectrum will be interpreted as the DOA of the real source. With the knowledge of the horizontal distance between the source and the array, the location of the real source can be calculated by coordinate transformation.

Some examples of location estimation error resulted from MUSIC with FBSS preprocessing under different combinations of SNR and source frequency are shown in Fig. 4. The percentage error of source location estimation is defined as the ratio between the error and the exact distance of the location from origin in percentage. The source is chosen to be located at long distance (y_s = 20 m) away from the array and 1 m above ground (near grazing propagation in Eq. (1)). As shown in Fig. 4, the location estimation in the x-direction generally gives a good approximation with error below 20% (i.e. < 0.1 m) under various condition of SNR regardless of the ground impedance (or flow resistivity). By comparing Figs. 4a(i), 4b(i), and 4c(i), it can be seen that the variation of ground impedance does not have significant impact on the source localization accuracy. It is also observed that the source frequency has no or limited effects on the location estimation in the x-direction. The performance is enhanced with reduced background noise level. Error decreases gradually as SNR increases from 0 to 20 dB, and reach a plateau at less than 10% (i.e. < 0.05m) for SNR above 20 dB.

The accuracy of source height estimation is affected by the strength of the ground reflection relative to the real source and their interference. Examples with abovementioned source-array geometry are used to illustrate the results of initial source height. The percentage error contours of location estimation in *z*-direction by MUSIC with σ_{eff} = 0.5 MNs/m^4 are shown in Fig. 4a(ii). Unlike the results obtained in *x*-direction (Fig. 4a(i)), the results in the *z*-direction deviate significantly from the desired value. The estimation with error > 100% is found at SNR < 0dB. It drops significantly to 40% at SNR > 10 dB for frequencies above 3 kHz. However, improvement is not observed when the background noise level is further reduced. Reduced error is found at higher source frequency because of the increased spatial resolution of the microphone array. Large error of the location estimation at low frequencies (below 2 kHz) is observed regardless of the SNR.

The strength of the ground reflection is affected by the ground impedance. This can be illustrated by comparing the source height estimation error patterns under different ground impedances (or flow resistivity) shown in Fig. 4. As the flow resistivity increases, the error of source height location estimation is improved in general at low frequencies for SNR > 10 dB. For instance, Fig. 4b(ii) shows the estimation error over a ground with σ_{eff} = 2 MNs/m^4, and the error is reduced at around 2 kHz and at frequency below 500 Hz for SNR > 10 dB compared with those at σ_{eff} = 0.5 MNs/m^4 shown in Fig. 4a(ii). Further reduction of error can be observed in this frequency range and SNR range as the flow resistivity is further increased to 30 MNs/m^4 as shown in Fig. 4c(ii).

The large error at σ_{eff} = 0.5 MNs/m^4 is believed to be the results of relatively large area of mutual cancelling between the direct source signal and the ground reflection as shown in Fig. 5a. It results in relatively weak signals picked up by the microphones as well as relatively uniform sound pressures across the 36 microphones. All of these lead to large error in the source height estimation by MUSIC after pre-processing. This phenomenon is much

improved when the sound frequency is increased and/or when the ground becomes more acoustically hard as shown in Figs. 5b and 5c respectively. Though sound pressure cancellations can still be found, especially in Fig. 5b, the sound pressure variations across the microphones have become significant.

Since the source and its image are on the same vertical plane, the phase variation of the signals in the *x*-direction can be easily scanned using by simple array signal processing technique. The estimation error in the *x*-direction is therefore much smaller, even in the presence of a background noise of similar magnitude.

The variations of error of the MUSIC source localization at *x*-direction is small as illustrated by the standard deviation (SD) maps of the corresponding estimation error shown in Fig. 6a(i). Larger variation of error is found at low SNR (< 20 dB) and low source frequencies (< 2 kHz). The SD decreases with increasing SNR and/or source frequency. A uniform SD at below 10% is found for SNR > 20 dB and source frequency above 2 kHz. Similar patterns have been found with other ground impedances tested as shown in Figs. 6b(i) and 6c(i).

The adverse effect of ground impedance on the source height estimation can further be revealed from the SD of the estimation error as shown in Fig. 6. Larger variation of the estimation error can generally be observed at σ_{eff} = 0.5 MNs/m^4 for SNR < 10 dB. As the flow resistivity increases, the SD variation is reduced at high frequencies as shown in Figs. 6b(ii) and 6c(ii). However, the SD of the error increases for SNR < 30 dB and source frequency below 2 kHz.

3.2. Results from Levenberg-Marquardt optimization

As mentioned in Section 2.2.1, the Levenberg-Marquardt (LM) method is useful in the parameter estimation for source localization and ground impedance estimation. A critical factor for a non-linear optimization method to be successful is the initial estimation of the

parameters. The results in Section 3.1 have demonstrated that MUSIC with FBSS method can provide a reasonable initial guess of source location for the application of the LM method in general.

With the results from MUSIC as the initial estimation of source location, the LM method is performed with $\lambda_d = 0.01$ and variable intervals for gradient estimation $dx = dy = 10^{-13}$ m and $d\sigma_{eff} = 100$ Ns/m^4. The estimations in the x-direction by LM method are illustrated in percentage error in Fig. 7a(i) with $\sigma_{eff} = 0.5$ MNs/m^4. Since the initial estimate of source location in the x-direction by MUSIC is reasonably accurate, the results in Fig. 7a(i) generally show similar pattern as that in Fig. 4a(i), but the error at low SNR (< 10 dB) and low frequencies (< 1.5 kHz) is increased, compared with results in Fig. 4a(i). The estimation error increases with flow resistivity for SNR < 10 dB and source frequency < 1.5 kHz as shown in Figs. 7b(i) and 7c(i) with $\sigma_{eff} = 2$ and 30 MNs/m^4, respectively. The SDs of the estimated error are slightly reduced using the LM method when both the flow resistivity, the SNR and source frequency are low, as shown in Fig. 8a(i), compared to that using solely MUSIC (Fig. 6a(i)). However, as the flow resistivity increases, variations of estimated error increase at low frequencies (< 1 kHz) regardless of the SNR (Figs. 8b(i) and 8c(i)).

The LM method shows significant improvement in the source height estimation, despite the unsatisfactory conditions discussed earlier in Section 3.1 (c.f. Fig. 4). For SNR < 10 dB, the error reduces from 80% to 40% at $\sigma_{eff} = 0.5$ MNs/m^4 as shown in Fig. 7a(ii). The percentage error is further reduced to less than 10% when the background noise level is further reduced. The relatively large error at around 1 kHz should be due to the signal cancelation by the coherent reflected sound. The error of source height estimation at low SNR (< 10 dB) and higher flow resistivity fluctuates as shown in Figs. 7b(ii) and 7c(ii). Relatively large error is also observed at around 5 kHz at $\sigma_{eff} = 30$ MNs/m^4, which is again due to the signal cancellation by the coherent reflected sound. The results show the potential

of LM method as an estimator of coherent source location using limited number of microphones. Improvement can be observed in the view of estimation error in source height determination. The map of SD for the estimation using LM method is shown in Fig. 8(ii). It can be found that the variation of error for height estimation has been significantly reduced over the entire frequency and SNR range at σ_{eff} = 0.5 and 2 MNs/m^4 (shown in Figs. 8a(ii) and 8b(ii), respectively (c.f. Figs. 6b(ii) and 6c(ii))). As the flow resistivity increases, further reduction of the error variation can be observed at low frequency and low SNR as shown in Fig. 8c(ii) at σ_{eff} = 30 MNs/m^4 (c.f. Fig. 6c(ii)). An observable decrease in estimation error in the presence of background noise is also found.

An important extension of using LM method is the possibility of ground surface impedance estimation (i.e. the spherical wave reflection coefficient, Q). Q is a function of variables including source-microphone geometry and normal ground surface impedance, Z. For a homogeneous ground surface, Q can be represented by Z (or normal ground surface admittance $\beta = 1/Z$). The results in the present study are presented in β instead of σ_{eff} for a closer representation of the ground effects.

The contour map of percentage of mean square error of the estimated ground surface admittance by LM method with the same source-receiver geometry as in the previous examples is shown in Fig. 9 for different types of ground surfaces. At low flow resistivity of 0.5 and 2 MNs/m^4, the estimation error of the real part of β gradually decreases as SNR increases but is less dependent on the source frequency as shown in Figs. 9a(i) and 9b(i). Error below 20% can be found for SNR above 20 dB. The corresponding results of the imaginary part of β are presented in Figs. 9a(ii) and 9b(ii). The mean errors for most scenarios are below 5%. The SD of the estimation error of β by the LM method is acceptable as can be observed from Figs. 10a(i) and (ii). The SD of the estimation error is below 20% for most cases, indicating that the repeatability of the estimation is satisfactory. The decrease

of SD is observed as SNR increases. As the flow resistivity increases, higher SD can be observed at low frequencies (< 1 kHz).

As the flow resistivity is further increased to 30 MNs/m^4, there is a dramatic jump of β estimation error at source frequency of ~4 kHz as shown in Figs. 9c(i) and 9c(ii). This jump is independent of the SNR, but its frequency depends significantly on the horizontal distance between the source and the receiver array, y_s, as shown in Fig. 11. It can be observed that this frequency of jump increases from ~1 kHz to ~2 kHz and ~4 kHz when y_s is increased from 5 m to 10 m and 20 m respectively in the presence of a relatively hard ground surface with σ_{eff} = 30 MNs/m^4. The frequency at which such jump is observed is hereinafter referred to as the jump frequency.

For a soft ground surface, the magnitude of Q in Eq. (1) is usually considerably less than unity because of sound absorption. However Q becomes close to unity when the reflecting ground becomes hard, such that serious interference between the source signal and the ground reflection is possible at some array microphone positions. Though complete destructive interference is still unlikely as $r_2 > r_1$, the signal interference will lead to large fluctuation of signal magnitude detected by the array microphones. The phase difference between the direct and the reflected sounds, Δ, as

$$\Delta = kr_2 + \angle Q - kr_1, \tag{211}$$

where $\angle Q$ is the phase angle of Q. Destructive interference occurs at $\Delta = \pi$.

Figure 12 illustrates the maps of $|\cos(\Delta)|$ at three sound frequencies near to the jump frequency of the case with x_s = 0.5 m, y_s = 5 m, z_s = 1 m and σ_{eff} = 30 MNs/m^4. At the frequency of 800 Hz, only one dark region with $\Delta = \pi/2$ is found (Fig. 12a). As the sound frequency increases, other dark region with $\Delta = 3\pi/2$ is found at the top of the microphone array (Fig. 12b). This region and also the one with $\Delta = \pi/2$ moves downwards as frequency

increases (Figs. 12b and 12c). The jump frequency is near to that at which the $\Delta = 3\pi/2$ dark region hits the uppermost microphone (#11). Similar observations can be made near to the other jump frequencies shown in Fig. 11. The β estimation using LM appears very unreliable in the presence of two regions on the microphone array in which the two interfering signals are of similar strengths and in a near-to-in-phase condition (i.e. Δ is in the fourth quadrant). The jump frequency therefore depends on the microphone arrangement in the measurement array. For a conservative estimation, one can take the frequency at which $\Delta = 3\pi/2$ at the uppermost microphone as the jump frequency.

Figure 13 shows the variation of the so-estimated jump frequency with y_s and σ_{eff} while all the other conditions are the same as those in Fig. 12. The jump frequency increases with increasing separation between the array and the source because of the reducing difference between r_1 and r_2. However, it should be noted that there are quite a number of microphones in the current measurement array setup which are located at approximately the same height as microphone #10, and thus the actual jump frequencies should be a bit higher than the predicted ones in Fig. 13. The higher the frequency is, the greater deviation this actual jump frequency from the predictions in Fig. 13 will be. The predicted jump frequency decreases with decreasing σ_{eff} (Fig. 13). However, the then more sound absorptive ground results in a larger reduction of the reflected sound strength. Thus, the above-observed jump at relatively hard ground does not occur (Fig. 9).

4. Conclusions

The acoustic inverse problem concerning a point harmonic source generating sound above a locally reactive ground surface has been studied. Source location and the ground surface impedance have been estimated by optimization of propagation model related parameters. The non-linear least square based method based on the Levenberg-Marquardt

method with the flexibility of handling parameters in different magnitude scales has been proposed for the estimation. The method is optimal with a close initial guess of the real sound source location. The MUSIC DOA algorithm with FBSS pre-processing scheme is suggested to provide such a robust initial guess of the source location.

Numerical simulation in frequency domain has been used to investigate the accuracy of the proposed method with artificial Gaussian white noise as background noise. A spatial random distributed planar array with 36 microphones is used as the receiver of the sound fields. The results of source localization at *x*-direction (i.e. horizontal direction) by MUSIC are satisfactory (error < 5%) for SNR above 10 dB. The interference between the direct sound and the ground reflection reduces the accuracy of MUSIC in estimating the source height. The problem becomes very serious when the two sounds tend to counteract with each other, resulting in weak signal pick-up and/or relatively uniform sound pressures in the microphone locations.

With the source locations estimated by MUSIC as initial inputs, the Levenberg-Marquardt method improves significantly the accuracy of source height estimation. The proposed method also provides flexibility of ground surface impedance estimation. Reliable results are obtained for SNR above 10 dB in general. However, large error in the ground surface impedance estimation is found when the direct sound and the ground reflection received at some microphones are of similar magnitudes and at near-to-in-phase condition. This happens when the ground is relatively hard. The highest frequency of reliable ground surface impedance estimation can be approximated by the frequency at which the phase difference of the interfering sounds at the uppermost microphone in the adopted sensing array is $3\pi/2$.

One should note that the effects of environmental conditions, such as temperature profile and turbulence, have not yet been taken into account in this study, so that the proposed method may not be ready for outdoor application. This is left to further investigation.

Acknowledgment

KCT was supported by a research studentship of the Hong Kong Polytechnic University.

References

[1] Y. Liu, A.P. Dowling, H.-C. Shin, Measurement and simulation of surface roughness noise using phased microphone arrays, *Journal of Sound and Vibration* 314 (1-2) (2008) 95 – 112.

[2] G.C. McLaskey, S.D. Glaser, C.U. Grosse, Beamforming array techniques for acoustic emission monitoring of large concrete structures, *Journal of Sound and Vibration* 329 (12) (2010) 2384 – 2394.

[3] J. Valin, F. Michaud, J. Rouat, Robust localization and tracking of simultaneous moving sound sources using beamforming and particle filtering, *Robotics and Autonomous Systems* 55 (3) (2007) 216 – 228.

[4] E. Tiana-Roig, F. Jacobsen, E.F. Grande, Beamforming with a circular microphone array for localization of environmental noise sources, *Journal of the Acoustical Society of America* 128 (6) (2010) 3535 – 3542.

[5] L. Du, L. Xu, J. Li, B. Guo, P. Stoica, C. Bahr, L.N. Cattafesta, Covariance-based approaches to aeroacoustic noise source analysis, *Journal of the Acoustical Society of America* 128 (5) (2010) 2877 – 2887.

[6] E. Sarradj, A fast signal subspace approach for the determination of absolute levels form phased microphone array measurements, *Journal of Sound and Vibration* 329 (9) (2010) 1553 – 1569.

[7] Y.I. Wu, K.T. Wong, X. Yuan, S.K. Lau, S.K. Tang, A directionally tunable but frequency-invariant beamformer on an acoustic velocity-sensor triad to enhance speech perception, *Journal of the Acoustical Society of America* 131 (5) (2012) 3891 – 3902.

[8] H. Kook, G.B. Moebs, P. Davies, J.S. Bolton, An efficient procedure for visualizing the sound field radiated by vehicles during standardized passby tests, *Journal of Sound and Vibration* 233 (1) (2000) 137 – 156.

[9] P. Jordon, J.A. Fitzpatrick, C. Meskell, Beampattern control of a microphone array to minimize secondary source contamination, *Journal of the Acoustical Society of America* 114 (4) (2003) 1920 – 1925.

[10] T. Yardibi, J. Li, P. Stoica, L.N. Cattafesta, Sparsity constrained deconvolution approaches for acoustic source mapping, *Journal of the Acoustical Society of America* 123 (5) (2008) 2631 – 2642.

[11] T. Yardibi, C. Bahr, N. Zawodny, F. Liu, L.N. Cattafesta, J. Li, Uncertainty analysis of the standard delay-and-sum beamformer and array calibration, *Journal of Sound and Vibration* 329 (13) (2010) 2654 – 2642.

[12] T.F. Brooks, W.M. Humphreys, A deconvolution approach for the mapping of acoustic source (DAMAS) determined from phased microphone arrays, *Journal of Sound and Vibration* 294 (4-5) (2006) 856 – 879.

[13] P. Gerstoft, W.S. Hodgkiss, Improving beampatterns of two dimensional random arrays using convex optimization, *Journal of the Acoustical Society of America* 129 (4) (2011) EL135 – 140.

[14] Y. Zhang, D. Sun, D. Zhang, Robust adaptive acoustic vector sensor beamforming using automated diagonal loading, *Applied Acoustics* 70 (8) (2009) 1029 – 1033.

[15] E. Habets, J. Benesty, I. Cohen, S. Gannot, J. Dmochowski, New insight into the MVDR beamformer in room acoustics, *IEEE Transactions on Audio, Speech, and Language Processing* 18 (1) (2010) 158 – 170.

[16] W. Pannert, Spatial smoothing for localized correlated sources – its effect on different localization methods in the nearfield, *Applied Acoustics* 72 (11) (2011) 873 – 883.

[17] P.A. Ravetta, R.A. Burdisso, W.F. Ng, Noise source localization and optimization of phased-array results, *American Institute of Aeronautics and Astronautics Journal* 47 (11) (2009) 2520 – 2533.

[18] D. Papamoschou, P.J. Morris, D.K. McLaughlin, Beamformed flow-acoustic correlations in a supersonic jet, *American Institute of Aeronautics and Astronautics Journal* 48 (10) (2010) 2445 – 2453.

[19] T. Suzuki, DAMAS2 using a point-spread function weakly varying in space, *American Institute of Aeronautics and Astronautics Journal* 48 (9) (2010) 2165 – 2169.

[20] V. Fleury, J. Bulté, Extension of deconvolution algorithms for the mapping of moving acoustic source, *Journal of the Acoustical Society of America* 129 (3) (2011) 1417 – 1428.

[21] H.C. Song, J. de Rosny, W.A. Kuperman, Improvement in matched field processing using the CLEAN algorithm, *Journal of the Acoustical Society of America* 113 (3) (2003) 1379 – 1386.

[22] E. Chang, Irregular array motion and extended integration for the suppression of spatial aliasing in passive sonar, *Journal of the Acoustical Society of America* 129 (2) (2011) 765 – 773.

[23] K. Ehrenfried, L. Koop, Comparson of iterative deconvolution algorithms for the mapping of acoustic sources, *American Institute of Aeronautics and Astronautics Journal* 45 (7) (2007) 1584 – 1595.

[24] B. Friedlander, A. Weiss, Direction finding using spatial smoothing with interpolated arrays, *IEEE Transactions on Aerospace and Electronic Systems* 28 (2) (1992) 574 – 587.

[25] J.S. Thompson, P.M. Grant, B. Mulgrew, Performance of spatial smoothing algorithms for correlated sources, *IEEE Transactions on Signal Processing* 44 (4) (1996) 1040 – 1046.

[26] Y.M. Chen, On spatial smoothing for two-dimensional direction-of-arrival estimation of coherent signals, *IEEE Transactions on Signal Processing* 45 (7) (1997) 1689 – 1696.

[27] Y.-H. Choi, Improved adaptive nulling of coherent interference without spatial smoothing, *IEEE Transactions on Signal Processing* 52 (12) (2004) 3464 – 3469.

[28] V.C. Anderson, P. Rudnick, Rejection of a coherent arrival at an array, *Journal of the Acoustical Society of America* 45 (2) (1969) 406 – 410.

[29] P.J. Kootsookos, D.B. Ward, R.C. Williamson, Imposing pattern nulls on broadband array responses, *Journal of the Acoustical Society of America* 105 (6) (1999) 3390 – 3398.

[30] E. Hoppe, M. Roan, Non-linear, adaptive array processing for acoustic interference suppression, *Journal of the Acoustical Society of America* 125 (6) (2009) 3835 – 3843.

[31] K.M. Li, K. Attenborough, N.W. Heap, Source height determination by ground effect inversion in the presence of a sound velocity gradient, *Journal of Sound and Vibration* 145 (1) (1991) 111 – 128.

[32] R. Kruse, S. Taherzadeh, The influence of environmental conditions on estimation of source distance and height using a single vertical array, *Applied Acoustics* 73 (2012) 198 – 208.

[33] J.F. Allard, B. Sieben, Measurement of acoustic impedance in a free field with two microphones and a spectrum analyzer, *Journal of the Acoustical Society of America* 77 (4) (1985) 1617 – 1618.

[34] S. Taherzadeh, K. Attenborough, Deduction of ground impedance from measurements of excess attenuation effects, *Journal of the Acoustical Society of America* 105 (3) (1999) 2039 – 2042.

[35] C. Nocke, V. Mellert, T. Waters-Fuller, K. Attenborough, K.M. Li, Impedance deduction from broad-band, point source measurements at grazing incidence, *Acustica united with Acta Acustica* 83 (6) (1997) 1085 – 1090.

[36] H.L. Van Trees, *Optimum Array Processing: Detection, Estimation, and Modulation Theory, Part IV*, Wiley, New York, 2002.

[37] K. Levenberg, A method for the solution of certain problems in least squares, *Quarterly of Applied Mathematics* 2 (2) (1944) 164 – 168.

[38] D. Marquardt, An algorithm for least-squares estimation of nonlinear parameters, *SIAM Journal on Applied Mathematics* 11 (2) (1963) 431 – 441.

[39] C.F. Chien, W.W. Soroka, Sound propagation along an impedance plane, *Journal of Sound and Vibration* 43 (1) (1975) 9 – 20.

[40] J.E. Fernández del Rio, M.F. Cátedra-Pérez, A comparison between matrix pencil and root-MUSIC for direction-of-arrival estimation making use of uniform linear array, *Digital Signal Processing* 7 (3) (1997), 153 – 162.

[41] N. Kanaya, Y. Iiguni, H. Maeda, 2-D DOA estimation method using Zernike moments, *Signal Processing* 82 (3) (2002) 521 – 526.

[42] K.M. Reddy, V.U. Reddy, Further results in spatial smoothing. *Signal Processing* 48 (3) (1996) 217 – 224.

[43] C. Vaidyanathan, K.M. Buckley, Performance analysis of DOA estimation based on nonlinear functions of covariance matrix, *Signal Processing* 50 (1) (1996) 5 – 16.

[44] T.J. Shan, M. Wax, T. Kailath, On spatial smoothing for direction-of-arrival estimation of coherent signals, *IEEE Transactions on Acoustics, Speech and Signal Processing* 33 (4) (1985) 806 – 811.

[45] M. Costa, A. Richter, V. Koivunen, DoA and polarization estimation for arbitrary array configurations, *IEEE Transactions on Signal Processing* 60 (5) (2012) 2330 – 2343.

[46] J.J. Christensen, J. Hald, *Beamforming – Technical review.* Brüel & Kjær, 2004.

[47] ANSI/ASA S.1.18, *Method for determining the acoustic impedance of ground surfaces.* American National Standard, 2010.

[48] M.E. Delany, E.N. Bazley, Acoustical properties of fibrous absorbent materials, *Applied Acoustics* 3 (2) (1970) 105 – 116.

[49] K. Attenborough, I. Bashir, S. Taherzadeh, Outdoor ground impedance models, *Journal of the Acoustical Society of America* 129 (5) (2011) 2806 – 2819.

Captions

Figure 1 Schematics of the present source-receiver system.

Figure 2 Flow chart of the proposed algorithm for parameter estimation in this study.

Figure 3 Microphone positions of the 36-channel arrays (relative to array centre).

● : Real array [46] ; ○ : virtual array for 500 Hz; ● : virtual array for 1200 Hz.

Figure 4 (Color online) Percentage error of source location estimation by MUSIC.

x_s = 0.5 m, y_s = 20 m, z_s = 1 m.

(a) σ_{eff} = 0.5 MNs/m^4; (b) σ_{eff} = 2 MNs/m^4; (c) σ_{eff} = 30 MNs/m^4;

(i) x-direction; (ii) z-direction.

Figure 5 (Color online) Interactions between direct sound and ground reflection.

x_s = 0.5 m, y_s = 20 m, z_s = 1 m.

(a) σ_{eff} = 0.5 MNs/m^4, 1000 Hz; (b) σ_{eff} = 0.5 MNs/m^4, 4000 Hz;

(c) σ_{eff} = 30 MNs/m^4, 1000 Hz;

Sub-figure : Numbering and positions of microphones.

○ : Real(source sound pressure); □ : Imag(source sound pressure);

● : Real(reflected sound pressure); ■ : Imag(reflected sound pressure).

——— : Real(overall sound pressure); — · — : Imag(overall sound pressure).

Figure 6 (Color online) Standard deviation of percentage error of source location estimation by MUSIC.

x_s = 0.5 m, y_s = 20 m, z_s = 1 m.

(a) σ_{eff} = 0.5 MNs/m^4; (b) σ_{eff} = 2 MNs/m^4; (c) σ_{eff} = 30 MNs/m^4;

(i) x-direction; (ii) z-direction.

Figure 7 (Color online) Percentage error of source location estimation by LM.

x_s = 0.5 m, y_s = 20 m, z_s = 1 m.

(a) σ_{eff} = 0.5 MNs/m^4; (b) σ_{eff} = 2 MNs/m^4; (c) σ_{eff} = 30 MNs/m^4;

(i) x-direction; (ii) z-direction.

Figure 8 (Color online) Standard deviation of percentage error of source location estimation by LM.

x_s = 0.5 m, y_s = 20 m, z_s = 1 m.

(a) σ_{eff} = 0.5 MNs/m^4; (b) σ_{eff} = 2 MNs/m^4; (c) σ_{eff} = 30 MNs/m^4;

(i) x-direction; (ii) z-direction.

Figure 9 (Color online) Percentage error of ground admittance estimation by LM.

x_s = 0.5 m, y_s = 20 m, z_s = 1 m.

(a) σ_{eff} = 0.5 MNs/m^4; (b) σ_{eff} = 2 MNs/m^4; (c) σ_{eff} = 30 MNs/m^4;

(i) Real(β); (ii) Imag(β).

Figure 10 (Color online) Standard deviation of percentage error of ground admittance estimation by LM.

x_s = 0.5 m, y_s = 20 m, z_s = 1 m.

(a) σ_{eff} = 0.5 MNs/m^4; (b) σ_{eff} = 2 MNs/m^4; (c) σ_{eff} = 30 MNs/m^4;

(i) Real(β); (ii) Imag(β).

Figure 11 (Color online) Effects of horizontal distance between source and receiver on the percentage error of ground impedance estimation by LM.

x_s = 0.5 m, z_s = 1 m; σ_{eff} = 30 MNs/m^4.

(a) y_s = 5 m; (b) y_s = 10 m; (c) y_s = 20 m;

(i) Real(β); (ii) Imag(β).

Figure 12 Phase difference variation across microphone array (Maps of $|\cos(\Delta)|$).

x_s = 0.5 m, y_s = 5 m, z_s = 1 m; σ_{eff} = 30 MNs/m^4.

(a) 800 Hz; (b) 1000 Hz; (c) 1200 Hz.

Circles : microphones; figures in circles : microphone number.

Figure 13 Variations of predicted jump frequency with y_s and σ_{eff}.

x_s = 0.5 m, z_s = 1 m;

——— : Hard ground; – – – – : σ_{eff} = 30 MNs/m^4;

— · — : σ_{eff} = 2 MNs/m^4; — · · — : σ_{eff} = 0.5 MNs/m^4.

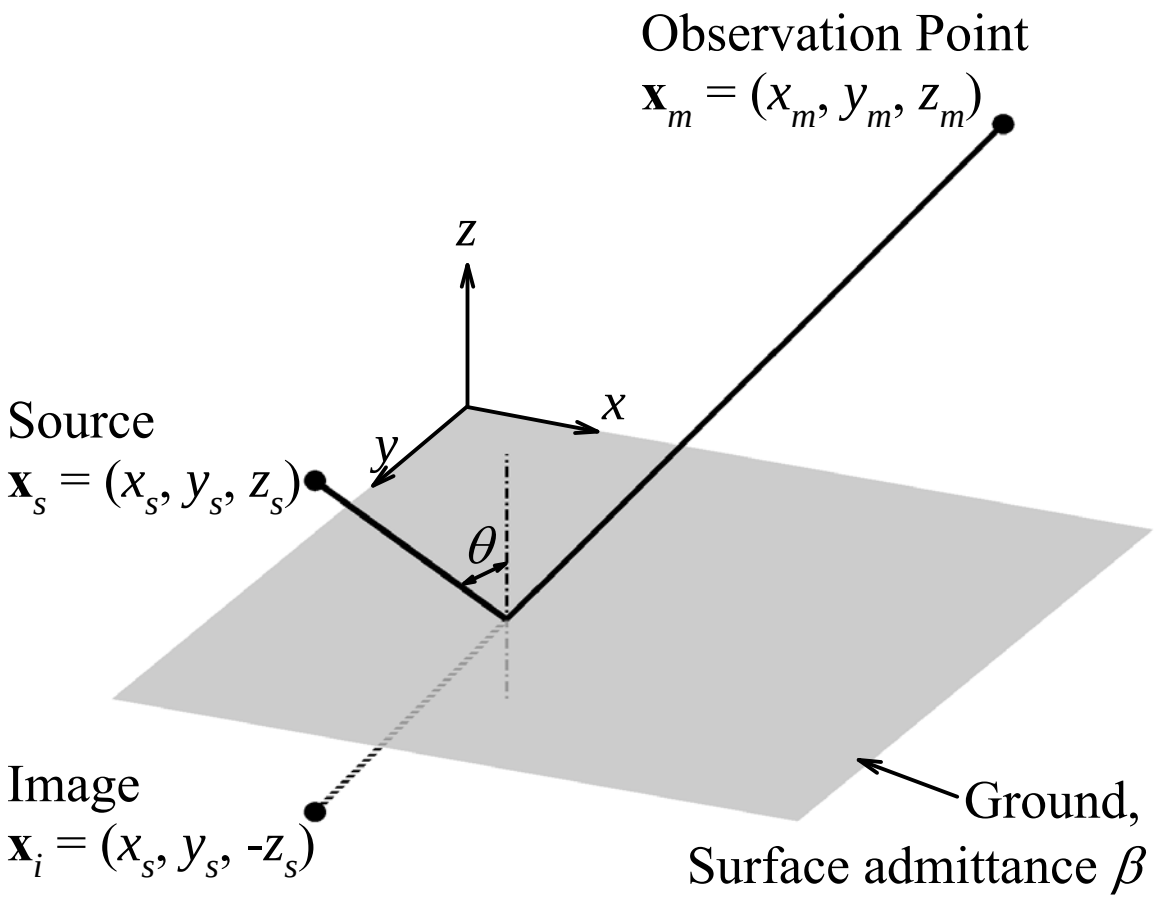
Observation Point
$\mathbf{x}_m = (x_m, y_m, z_m)$
z
x
y
Source
$\mathbf{x}_s = (x_s, y_s, z_s)$
θ
Image
$\mathbf{x}_i = (x_s, y_s, -z_s)$
Ground,
Surface admittance β

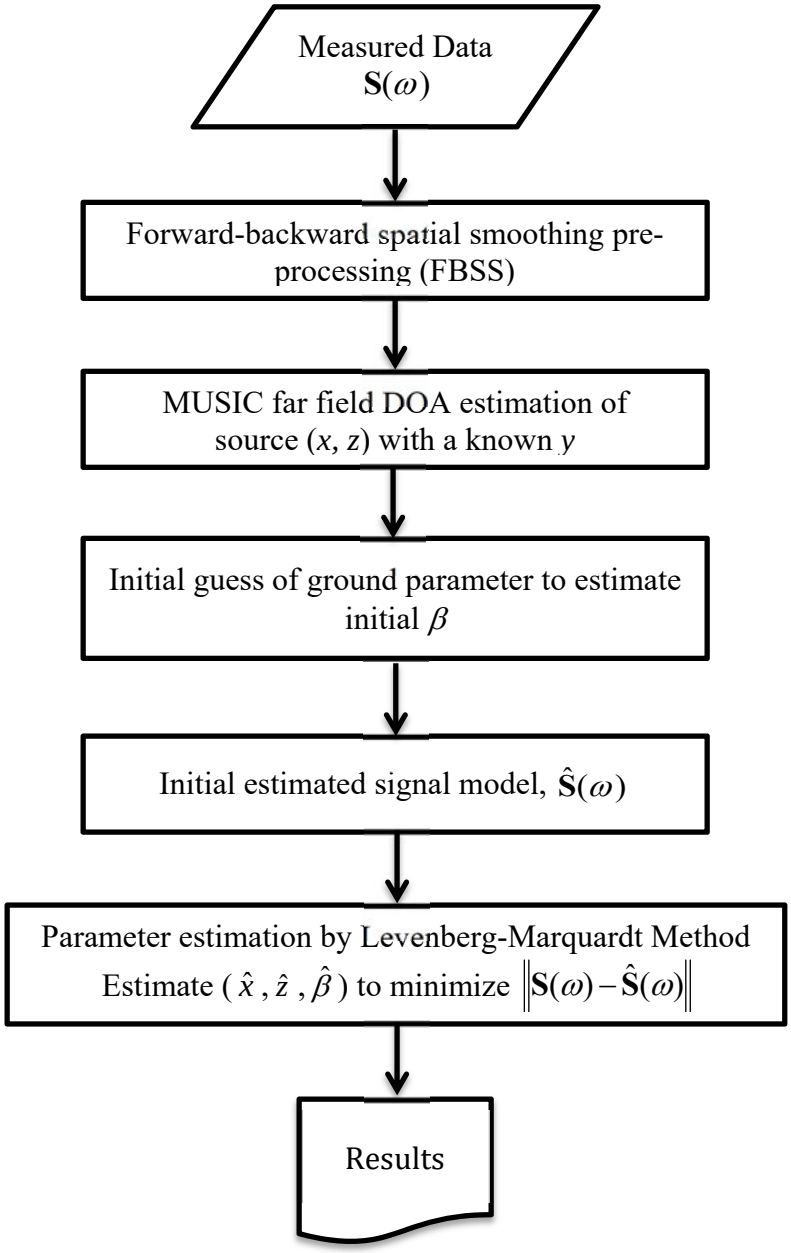
Measured Data
$\mathbf{S}(\omega)$
Forward-backward spatial smoothing pre-processing (FBSS)
MUSIC far field DOA estimation of source (x, z) with a known y
Initial guess of ground parameter to estimate initial β
Initial estimated signal model, $\hat{\mathbf{S}}(\omega)$
Parameter estimation by Levenberg-Marquardt Method
Estimate ($\hat{x}$, $\hat{z}$, $\hat{\beta}$) to minimize $\|\mathbf{S}(\omega)-\hat{\mathbf{S}}(\omega)\|$
Results

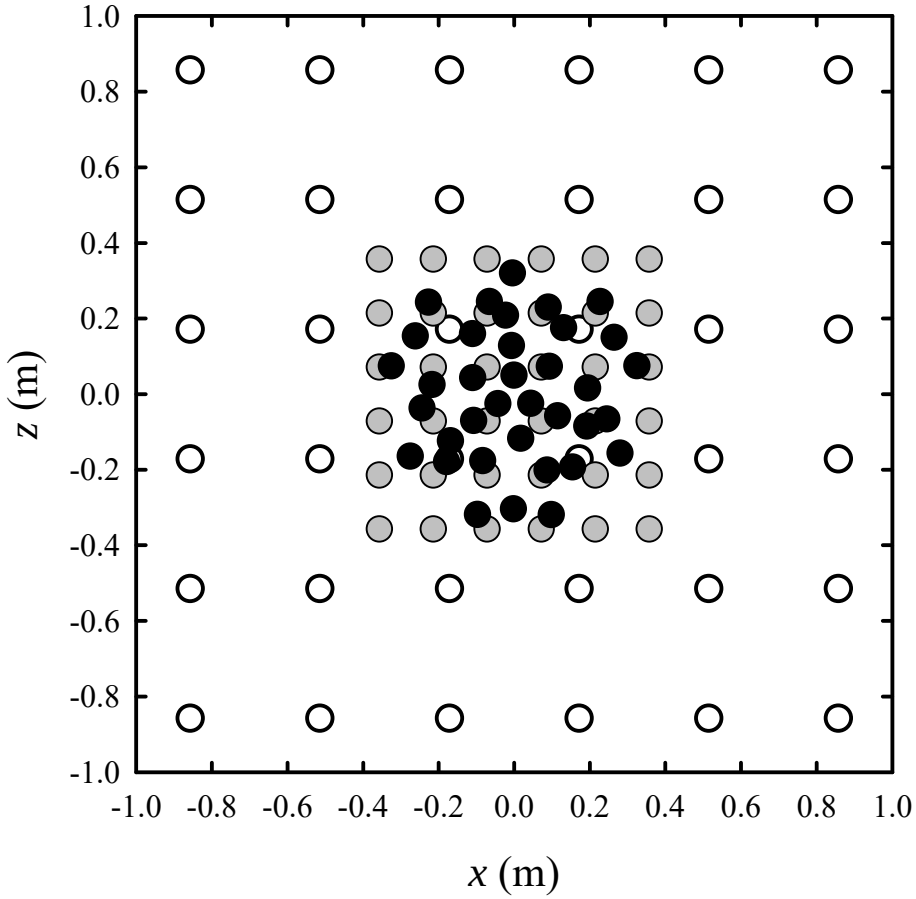
1.0
0.8
0.6
0.4
0.2
0.0
-0.2
-0.4
-0.6
-0.8
-1.0
z (m)
-1.0 -0.8 -0.6 -0.4 -0.2 0.0 0.2 0.4 0.6 0.8 1.0
x (m)

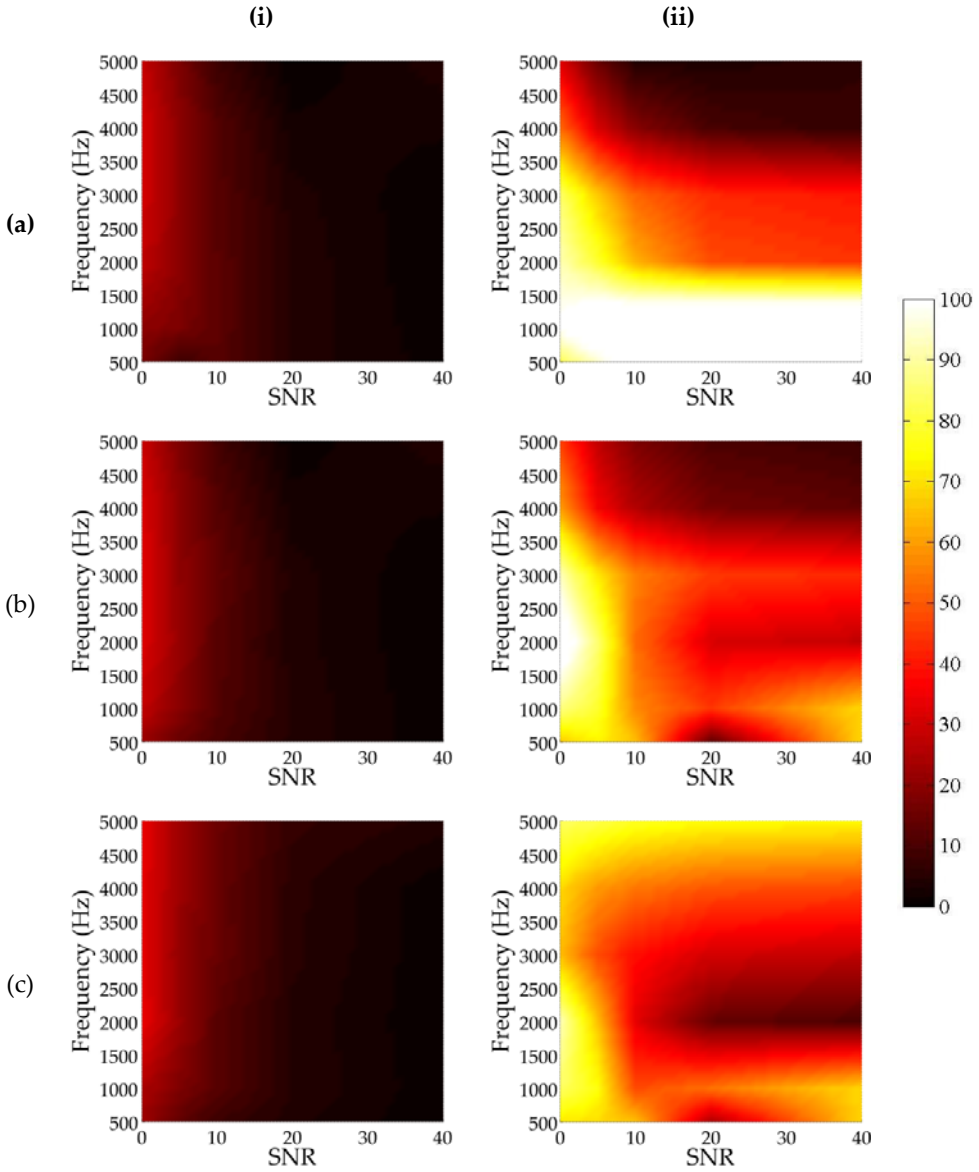
(i)
(ii)
(a)
(b)
(c)
Frequency (Hz)
SNR
5000
4500
4000
3500
3000
2500
2000
1500
1000
500
0
10
20
30
40
100
90
80
70
60
50
40
30
20
10
0

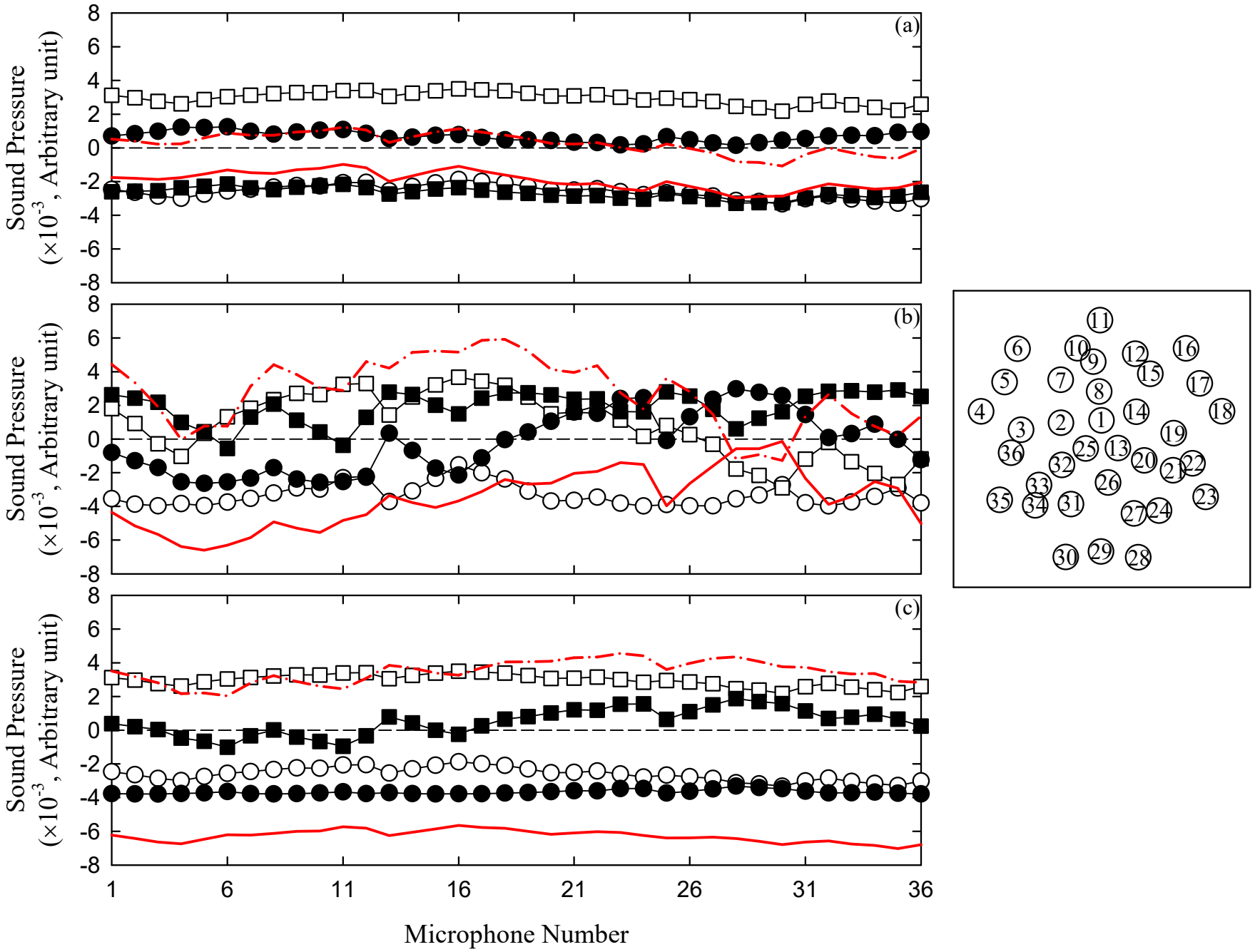
(a)
(b)
(c)
Sound Pressure
(×10^-3, Arbitrary unit)
8
6
4
2
0
-2
-4
-6
-8
1
6
11
16
21
26
31
36
Microphone Number
11
6
10
9
12
16
5
7
15
17
8
4
14
18
3
2
1
19
36
25
13
20
21
22
32
33
26
35
34
31
27
24
23
30
29
28

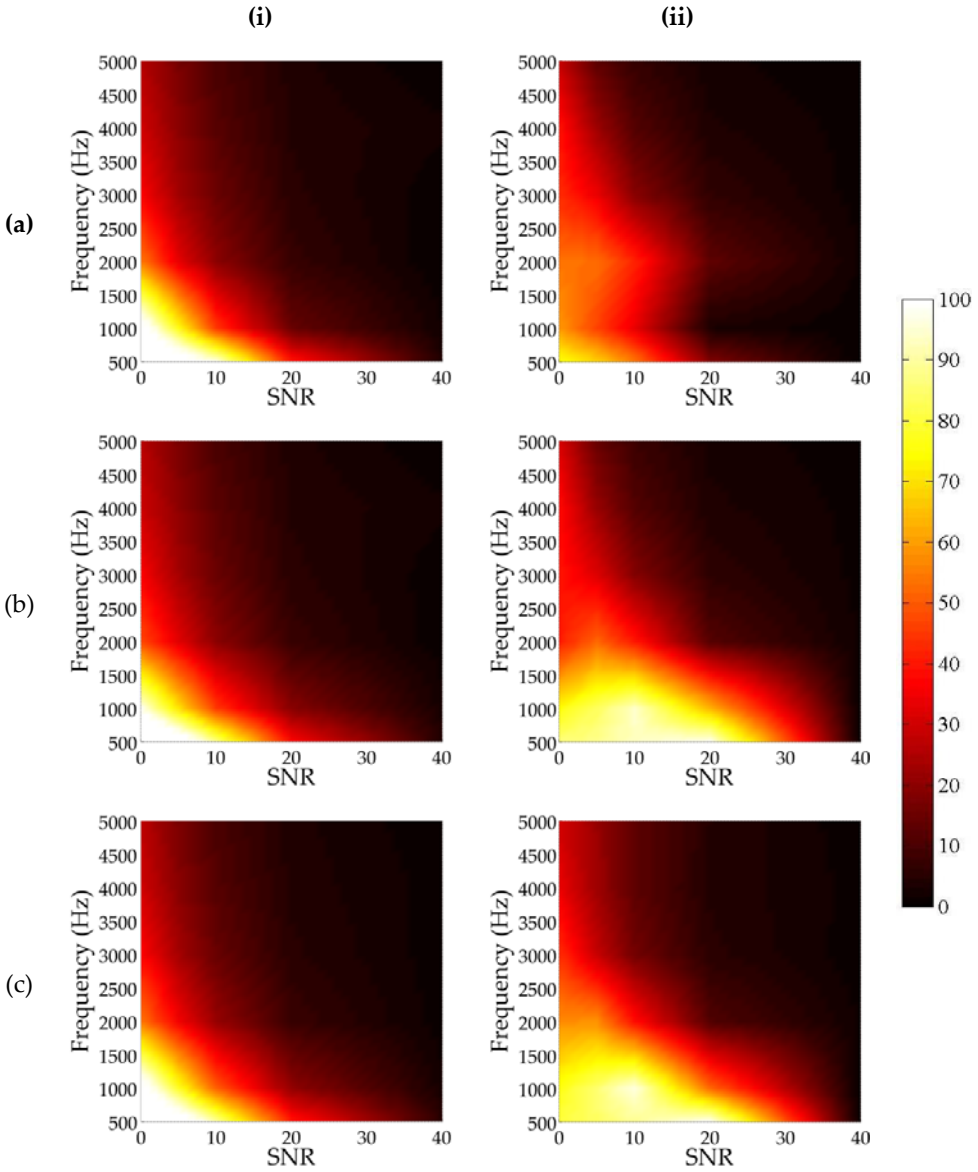
(i)
(ii)
(a)
(b)
(c)
Frequency (Hz)
SNR
5000
4500
4000
3500
3000
2500
2000
1500
1000
500
0
10
20
30
40
100
90
80
70
60
50
40
30
20
10
0

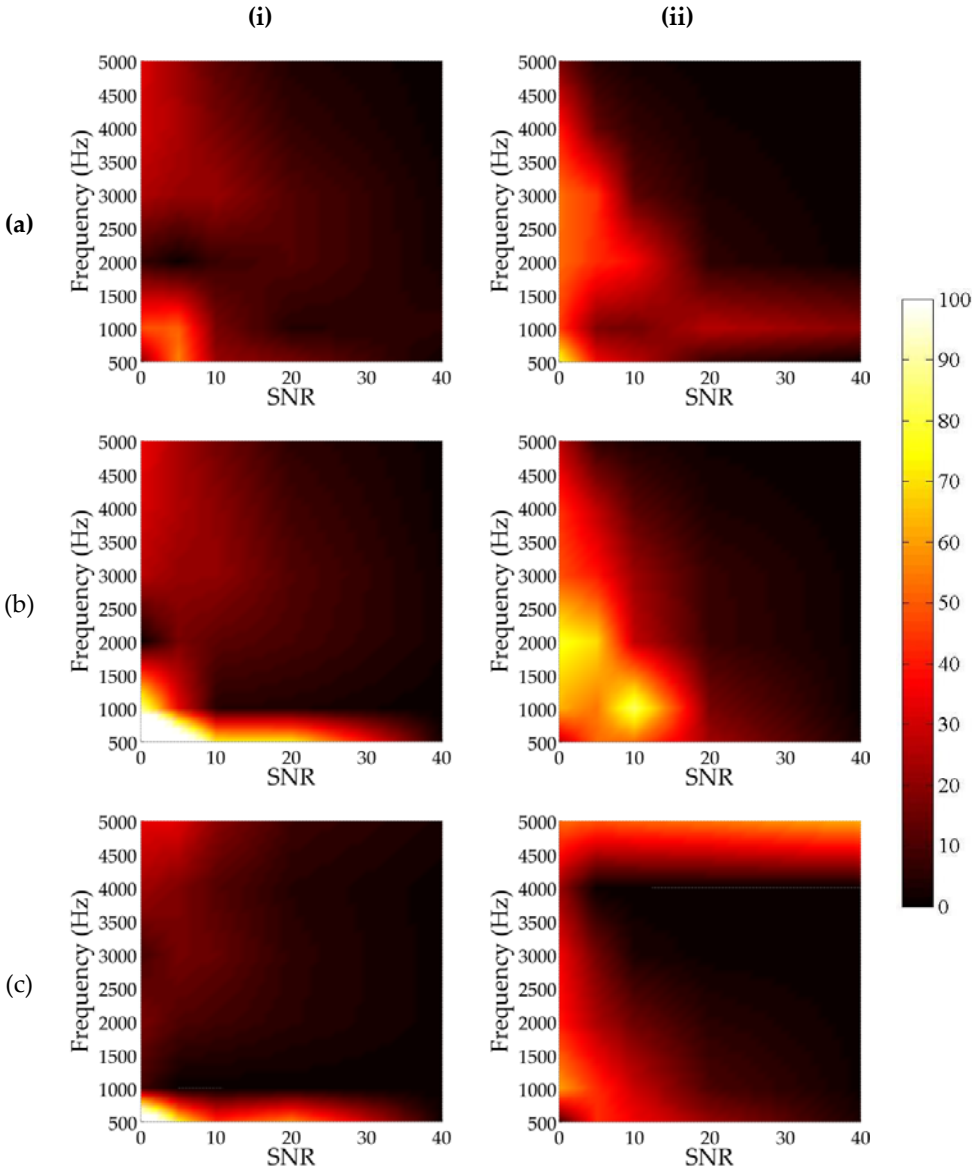
(i)
(ii)
(a)
(b)
(c)
Frequency (Hz)
SNR
5000
4500
4000
3500
3000
2500
2000
1500
1000
500
0
10
20
30
40
100
90
80
70
60
50
40
30
20
10
0

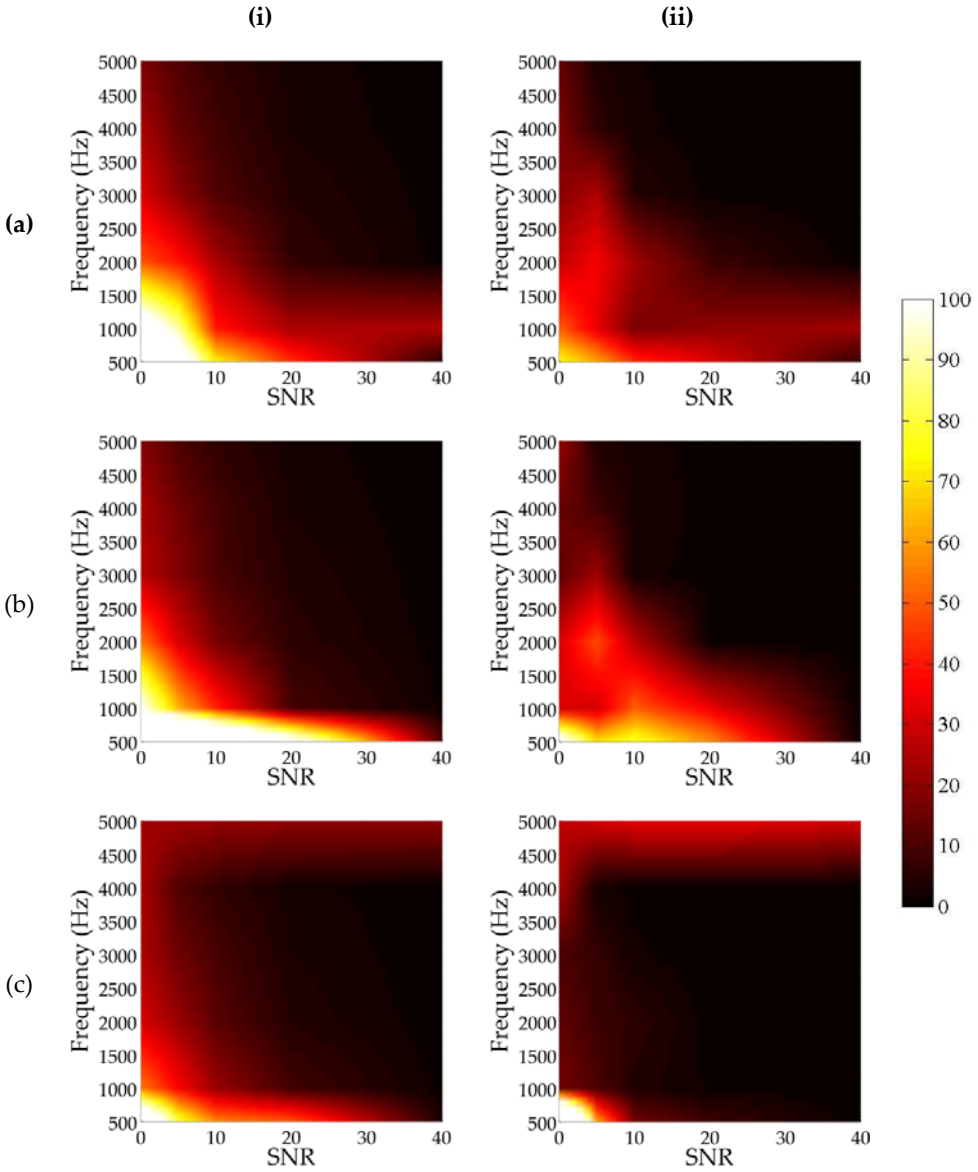
(i)
(ii)
(a)
(b)
(c)
Frequency (Hz)
SNR
5000
4500
4000
3500
3000
2500
2000
1500
1000
500
0
10
20
30
40
100
90
80
70
60
50
40
30
20
10
0

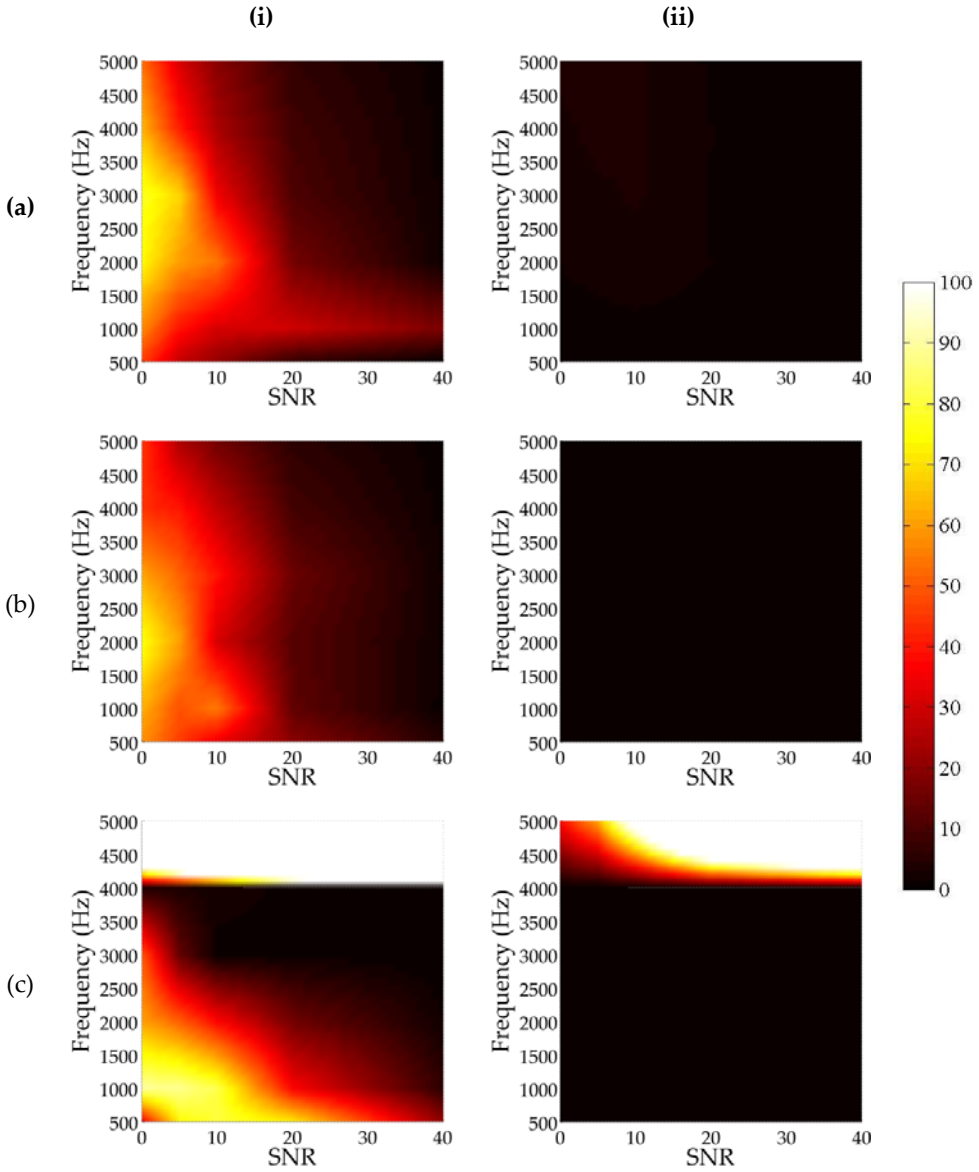
(i)
(ii)
(a)
(b)
(c)
Frequency (Hz)
SNR
5000
4500
4000
3500
3000
2500
2000
1500
1000
500
0
10
20
30
40
100
90
80
70
60
50
40
30
20
10
0

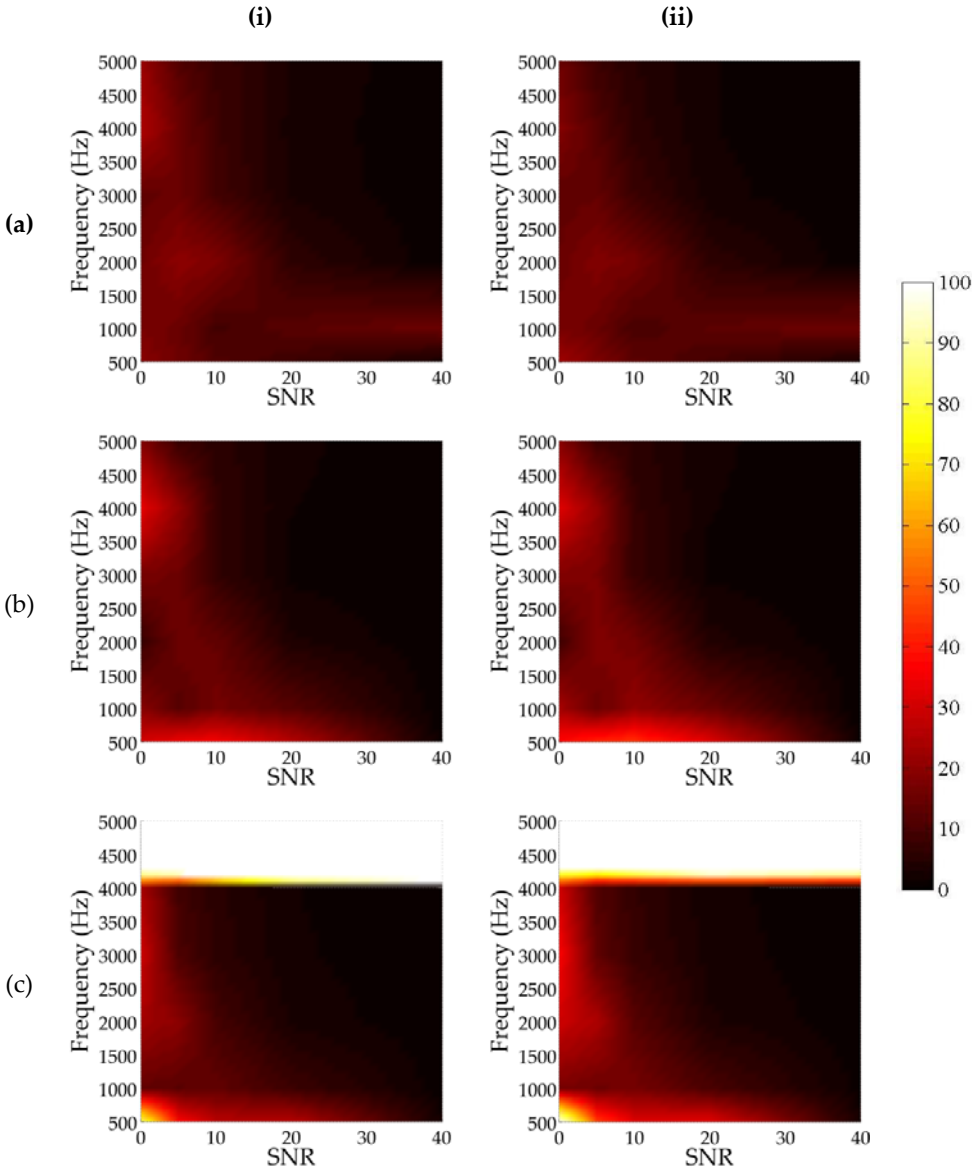
(i)
(ii)
(a)
(b)
(c)
Frequency (Hz)
SNR
5000
4500
4000
3500
3000
2500
2000
1500
1000
500
0
10
20
30
40
100
90
80
70
60
50
40
30
20
10
0

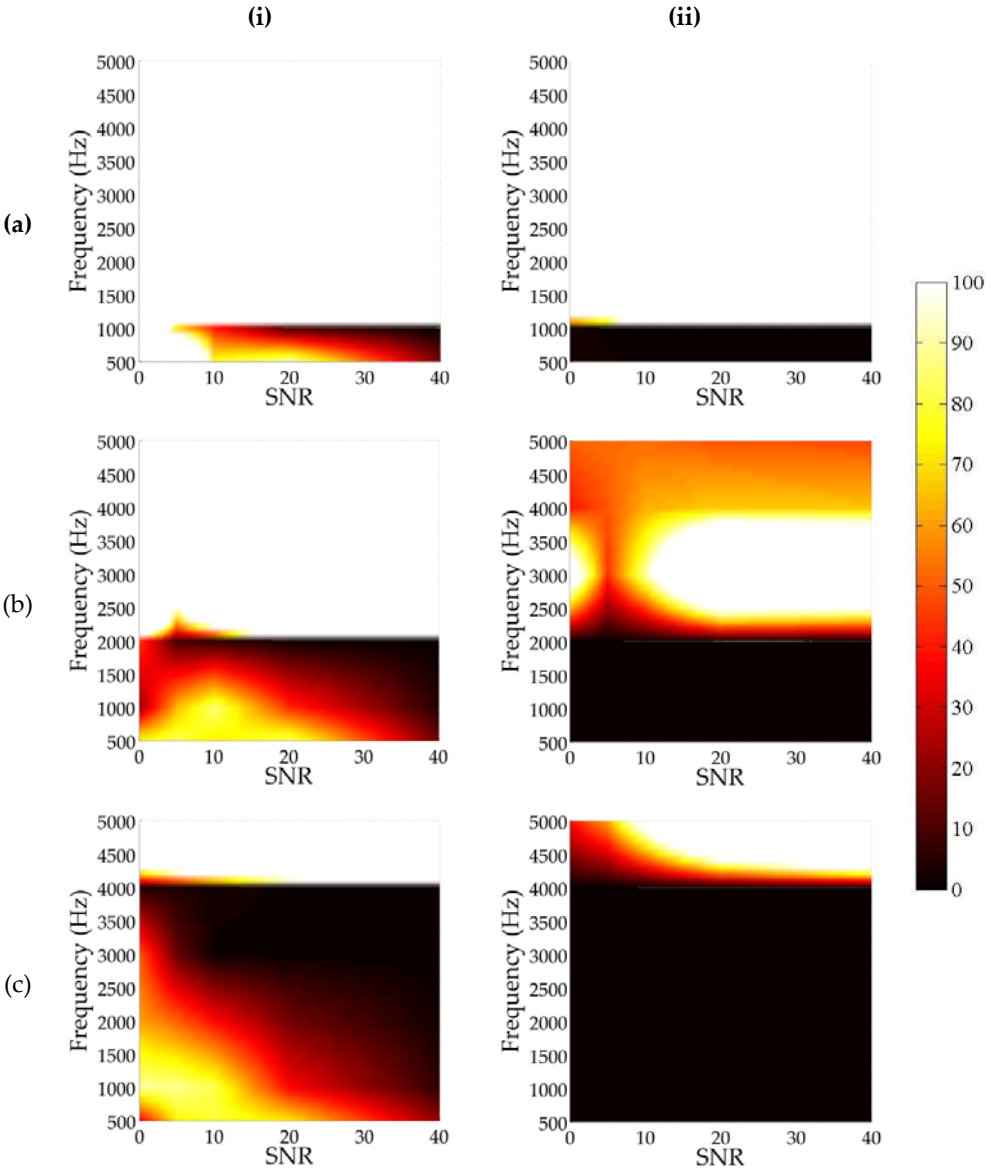
(i)
(ii)
(a)
(b)
(c)
Frequency (Hz)
SNR
5000
4500
4000
3500
3000
2500
2000
1500
1000
500
0
10
20
30
40
100
90
80
70
60
50
40
30
20
10
0

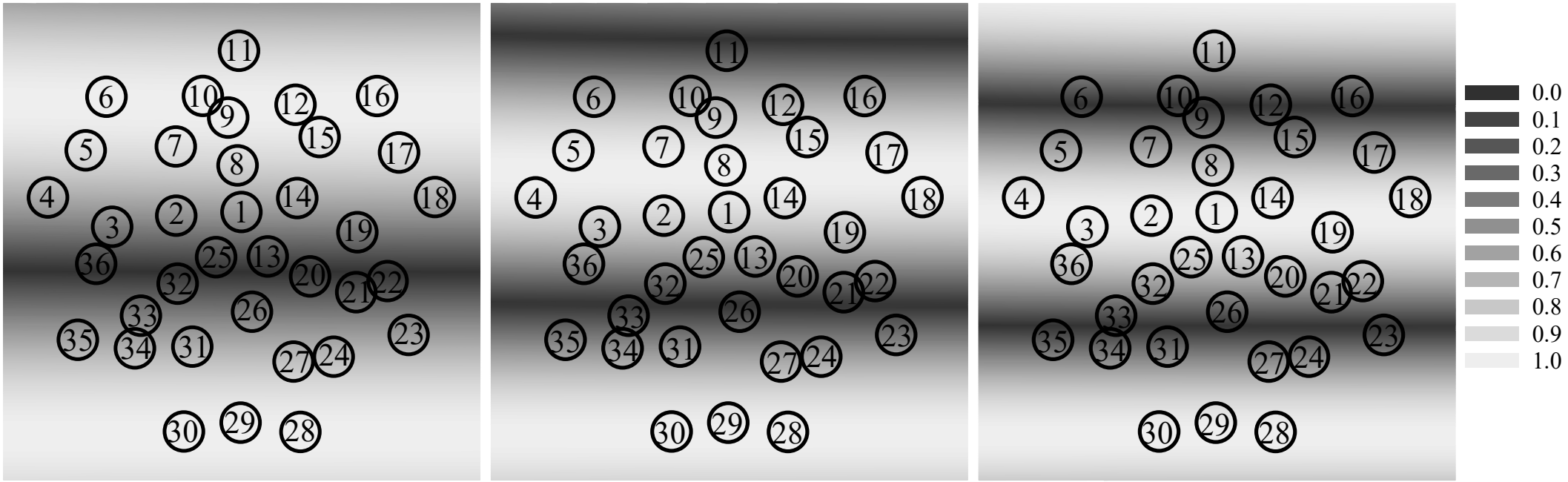
11
6
10
9
12
16
5
7
15
17
8
4
14
18
3
2
1
19
36
25
13
20
21
22
32
26
33
23
35
34
31
27
24
30
29
28
0.0
0.1
0.2
0.3
0.4
0.5
0.6
0.7
0.8
0.9
1.0

(a) (b) (c)

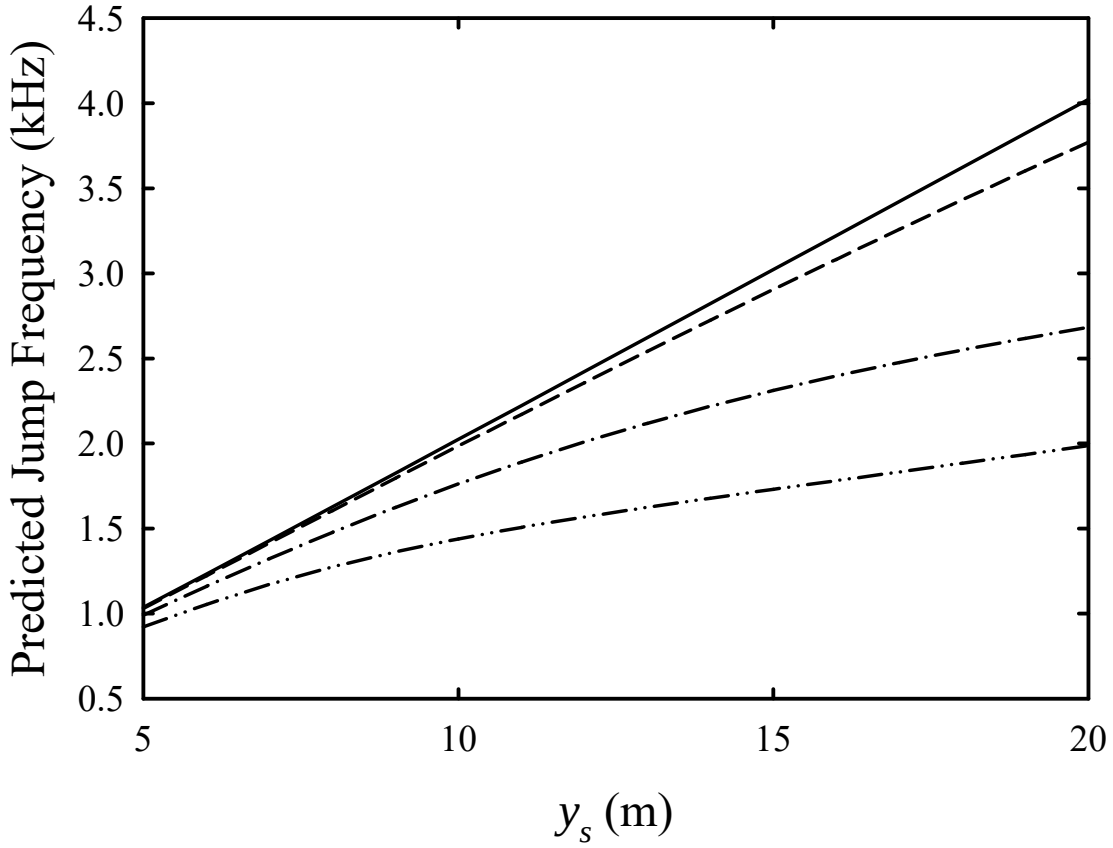
Predicted Jump Frequency (kHz)
4.5
4.0
3.5
3.0
2.5
2.0
1.5
1.0
0.5
5
10
15
20
y_s (m)